Energy Storage Materials 24 (2020) 265–271

Contents lists available at ScienceDirect

Energy Storage Materials

journal homepage: www.elsevier.com/locate/ensm

Dendrite–free and Ultra–High energy lithium sulfur battery enabled by dimethyl polysulfide intermediates

Jie Liu, Tao Qian **, Na Xu, Mengfan Wang, Jinqiu Zhou, Xiaowei Shen, Chenglin Yan *

College of Energy, Key Laboratory of Advanced Carbon Materials and Wearable Energy Technologies of Jiangsu Province, Soochow University, Suzhou, 215006, China

ARTICLE INFO

Keywords:
Lithium sulfur battery
Discharge intermediates
High energy density
In–situ UV/Vis spectroscopy

ABSTRACT

Although lithium sulfur batteries made a lot of progress over decades, they are still faced with low energy and fragile stability. Herein, we report a new strategy to achieve extremely high energy lithium sulfur battery with dimethyl polysulfide intermediates, which can greatly increase the specific capacity to 1497.3 mAh g^{-1} at 0.1C, and dendrite–free lithium anode so as to ensure a long lifespan with 500 cycles. The brilliant performance is attributed to the radical exchange between sulfur and dimethyl polysulfide intermediates rather than lithium polysufides. Density functional theory calculations and nuclear magnetic resonance spectroscopy verify the existence of dimethyl polysulfide intermediates and *in–situ* UV/Vis spectroscopy confirms that mechanism for exchange reaction of radicals can boost the capacity of sulfur cathodes by eliminating complications, such as shuttle effect associated with formation and transformation of lithium polysulfides in the electrolyte. This study develops a new avenue for the innovative discharge intermediate design that helps increase capacity and stability for the practical application of lithium sulfur batteries.

1. Introduction

Although lithium sulfur (Li–S) batteries, which use elemental sulfur abundantly in nature as the cathode material, have garnered a great deal of attention attributed to their unique advantages in gravimetric energy density (2600 W h kg^{-1}) compared to conventional lithium batteries and gradually help human beings to get rid of the dependence on traditional energy, they still can't accommodate the practical applications as energy storage devices [1–7]. The common Li–S batteries have complex redox reactions involving multiple electrons accompanying morphology and phase transitions upon cycling [8–10]. Moy et al. deduced a theoretical model to analyze the multistep discharge mechanism of Li–S cell [8,11]. The conversion process from sulfur to long–chain polysulfides corresponds to the higher plateau (2.15–2.4 V) in the voltage profile of conventional Li–S batteries, and the lower plateau at ~ 2.1 V attributes to the formation of insoluble Li_2S_2 and Li_2S [3,12,13]. These complex reactions lead to a low Coulombic efficiency and the fading of capacity since S_x^{2-} ($4 \leq x \leq 8$) is soluble in the organic liquid electrolyte and can gradually diffuse out of the cathode region (shuttle effect). Other impediments, such as inherent non–conduction character of sulfur and lithium sulfide and the remarkable volumetric expansion (over 80% from S to Li_2S) during lithiation, are also urgent to be solved [3,14–16].

Recently, we have witnessed Li–S batteries with partly improved capacity enabled by modified electrodes [17–21], but the issue that maintains stability, especially at high capacity, has still not been resolved yet. Several efficient approaches have been presented to improve the cycle performance, including the encapsulation of sulfur with various carbon matrixes [22–24] and adsorbing the soluble polysulfides on the surface of electrode [25–27], but the weak absorption just restrained the diffusion of long–chain polysulfides (Li_2S_x, $4 \leq x \leq 8$) in a short period of time and the polysulfides may eventually diffuse to the anode since conventional strategies failed to figure out the fundamental issue on the generation of polysulfides. It is a tough assignment to maintain an excellent stability with a high capacity in Li–S battery.

The development of new cathodes attracts most attentions but few realize that the electrolytes, a much higher proportion than cathode and anode materials in weight, can be utilized to improve the overall capacity and cycle performance. In order to drive Li–S battery research to practical applications, some other strategies should be proposed to integrate with the currently developed Li–S systems. Herein, we realized a bran–new concept aimed to increase the cell capacity and cycle performance by forming dimethyl polysulfide rather than lithium polysulfides as

** Corresponding author.
* Corresponding author.
E-mail addresses: tqian@suda.edu.cn (T. Qian), c.yan@suda.edu.cn (C. Yan).

https://doi.org/10.1016/j.ensm.2019.08.010
Received 13 March 2019; Received in revised form 16 July 2019; Accepted 9 August 2019
Available online 14 August 2019

discharging intermediates. According to density functional theory (DFT) calculations of Gibbs free energy, dimethyl trisulfide (DMTS) is the most stable form in dimethyl thioether system. During cycling, DMTS occurs as radical $CH_3SS\bullet$ and $CH_3S\bullet$ in the electrolyte system and the sulfur existed in radicals participated in the radical exchange reaction to form dimethyl polysulfide intermediates. Quite different from the conventional Li–S battery, the as–prepared cell in new electrolyte shows only one discharge plateau at ~2.06 V as seen in the voltage profiles, indicating the absence of soluble lithium polysulfides during battery cycling [12,13]. Moreover, the well–assembled battery presents an ultrahigh specific capacity of 1497.3 mAh g^{-1} at 0.1C (1C = 1675 mA g^{-1}, based on sulfur weight), and the dendrite–free lithium deposition guarantees excellent capacity retention over 84.1 % after 500 cycles. *In–situ* UV/Vis spectroscopy and ^{1}H nuclear magnetic resonance spectroscopy (^{1}H NMR) are used to validate the reduction pathway and possible mechanism for lithiation and delithiation processes in the novel system, and the results are well consistent with electrochemical results, which provide a logical theoretical explanation on the increase of capacity retention.

2. Experimental section

2.1. Electrolyte preparation and cell fabrication

The conventional electrolyte was prepared by dissolving 1 M lithium bis(trifluoromethanesulfonyl) imide (LiTFSI) into 1,2–dimethoxyethane (DME) and 1,3–dioxolane (DOL) (v/v, 1:1). The DMTS modified electrolytes were prepared similarly except altering the ratio of DMTS in DME/DOL from 10 to 40 vol%. Besides, to improve the cycling efficiency, 1% $LiNO_3$ additive was added to all the electrolytes.

2.2. Preparation of S/C composites

The composites of S/C were manufactured by the direct impregnation of sulfur into the carbon frameworks. Briefly, 150 mg sulfur and 50 mg carbon was ball–milled at 800 rpm for 4 h. The mixture was transferred into a 10 mL PTFE reaction kettle and sealed in argon atmosphere. After 160 °C for 10 h, the obtained products were collected.

2.3. Characterization

The *in–situ* UV/Vis Spectroscopy was operated on a UV Lambda 750 UV/Vis/NIR spectrometer. Punching a 10 mm hole at the central of lithium wafer and cathode, the well–designed cell was encapsulated like other tested cells except replacing the Celgard 2400 separators with Whatman Glass–Fiber separators. Notably, the punched cathode should be sealed by an optical glass cover to form a window, which was no effect on the transmitting of light. The ^{1}H NMR was carried on a 300 MHz superconducting nuclear magnetic resonance spectrometer (^{1}H NMR, NMRststem, USA). We encapsulated five batteries in an Ar–filled glove box and kept the assembly conditions as same as possible. Cycling these cells in the glove box and disassembling the cell in sequence when it discharged to designated potential. All the separators picked from disassembled cells discharged to different potentials were immersed in 700 μl $CDCl_3$. Both the cells for NMR and UV/Vis spectroscopy analysis were cycled in 30 vol% DMTS modified electrolyte rate with 3.0–4.0 mg cm^{-2} of sulfur loading.

2.4. Electrochemical characterization

Electrochemical characterization of S/C in different electrolytes was performed in 2025 coin–type cells. The working electrodes were prepared by dispersing 85 wt% active materials, 5 wt% acetylene black, and 10 wt% polyvinylidene difluoride in NMP and thoroughly mixing. The mixed slurry was casted onto Al–foil current collector by a doctor–blade method. After vacuum drying at 60 °C for 24 h, the electrodes were punched into discs (Φ = 12 mm, 1.13 cm^2). The sulfur loading in every electrode was about 1.0 mg. The electrodes were assembled in an Ar–filled glove box with pure Li foil as the counter, where conventional electrolyte and DMTS–containing electrolytes in different proportion were respectively used as the electrolyte. All the cells contained a same content of electrolyte (25 μL). The charge–discharge properties and cyclic voltammetric were tested on the CT2001A cell test instrument (Wuhan LAND Electronic Co., Ltd) and CHI660E (Shanghai Chenhua instrument Co., Ltd) electrochemical workstation, respectively. The specific capacities were based on the mass of sulfur powder in cathode electrodes and removed the contribution of DMTS, which were calculated by the formula: C = (The overall capacity – The capacity contributed by DMTS)/ the mass of sulfur powder.

2.5. Computational methods

The rb3lyp density functional method was employed in this work to carry out all the computations. The 6–31G(d + p) basis set was used for all the atoms in the geometry optimizations. Vibrational frequency analyses at the same level of theory were performed on all optimized structures to characterize stationary points as local minima or transition states. The Gaussian 09 suite of programs was used throughout.

3. Results and discussion

We started from DFT calculations to design the experiments, and $CH_3S_nCH_3$ ($2 \le n \le 7$) and sulfur radicals were taken as the model system to evaluate the stability of $CH_3S_nCH_3$ where n was in different values (Fig. 1a). According to the Gibbs free energy in following reactions (vacuum conditions),

$$CH_3SSCH_3 + S \rightleftharpoons CH_3SSSCH_3,\ \Delta G_1 = -3.93\ \text{J/mol} \quad (1)$$

$$CH_3SSSCH_3 + S \rightleftharpoons CH_3SSSSCH_3,\ \Delta G_2 = 4.23\ \text{J/mol} \quad (2)$$

$\Delta G_1 < 0$ and $\Delta G_2 > 0$ indicated that CH_3SSSCH_3 would exist in a stable state in the system. Similarly,

$$CH_3S_4CH_3 + S \rightleftharpoons CH_3S_5CH_3,\ \Delta G_3 = 2.57\ \text{J/mol} \quad (3)$$

$$CH_3S_5CH_3 + S \rightleftharpoons CH_3S_6CH_3,\ \Delta G_4 = 3.73\ \text{J/mol} \quad (4)$$

and the results of ΔG_3 and ΔG_4 suggested that the generation of $CH_3S_5CH_3$ and $CH_3S_6CH_3$ were even harder. The same conclusion can be obtained when setting DOL and DME as the solvents to simulate the organic electrolyte environment, respectively (Table S1). We chose DMTS as an additive to complete a reversible electrochemical reaction as DMTS was the most stable form. DMTS had a unique thioether structure featured with multielectron reduction reactions during cycling, which made great contribution to the increase of cell capacity. Simply, the additional capacity of 851 mAh g^{-1} can be attributed to the following reaction:

$$CH_3SSSCH_3 + 4Li^+ + 4e^- \rightleftharpoons 2CH_3SLi + Li_2S \quad (5)$$

The differences of electrochemical behaviors between conventional DME/DOL electrolytes and DMTS modified electrolytes are shown in Fig. 2. As shown in galvanostatic discharge/charge voltage profiles in Fig. 2a, the S/C cathode in traditional electrolyte shows two typical discharge plateaus (~2.32 V and 2.10 V), which are associated with sulfur reduction to long–chain polysulfides and a further conversion to short–chain sulfides, respectively [3,13]. However, only one plateau, at ~2.08 V, is prominent in the cell based on DMTS additive electrolyte. It means that in this system, DMTS plays a part in preventing sulfur active materials from achieving its routine, forming Li_2S_x ($4 \le x \le 8$) at the final discharge state. Moreover, a small gap between discharge and charge curves illustrates that the DMTS system exhibits faster redox kinetics than that in the conventional electrolyte [28]. The similar conclusion can also be drawn from the comparison of cyclic voltammogram (CV) curves of two different cells, which are measured in the voltage range of

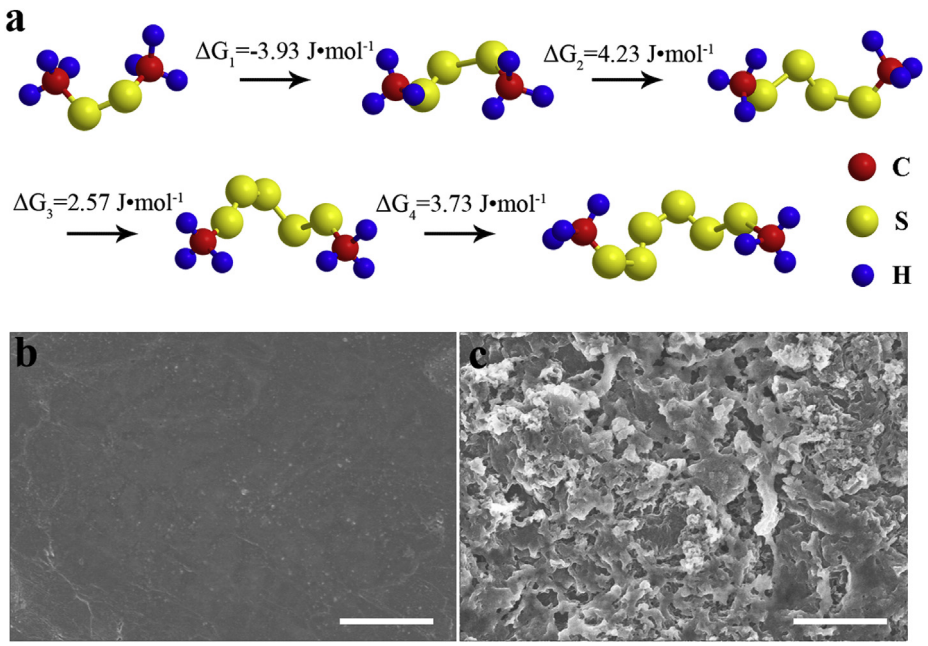

Fig. 1. (a) Gibbs free energy in chain extension reactions of $CH_3S_nCH_3$ ($2 \leq n \leq 6$) from DFT calculations, which demonstrates that DMTS existed in the most stable state in dimethyl thioether system. (b) In DMTS modified cell, the lithium surface exhibits uniform morphology without the indication of lithium dendrites after 500 cycles, contrasting to intricate lithium dendrites and cracks in (c) conventional DME/DOL cell. Scale bar, 50 μm.

1.6–2.8 V at a scan rate of 0.1 mV s^{-1} (Fig. 2b). Considering that the activation phenomenon always appears in the first cycle, the curves of the second cycle of these two cells are chosen to compare the different potentials where the redox reaction occurs [29,30]. There is only one cathodic peak at 2.06 V in the cell with DMTS modified electrolyte, as compared to the two peaks at 2.35 V and 2.06 V in the pure DME/DOL system, which correspond to the two–step reduction process of element sulfur in cyclic form [15,29]. A tremendous difference in specific capacity and cycle performance between DMTS modified and conventional Li–S batteries can be seen in Fig. 2c. Specifically, the initial discharge capacity of 1497.3 mAh g^{-1} in 30 vol% DMTS modified electrolyte is obtained at a rate of 0.1C, which is much higher than the capacity of 949.6 mAh g^{-1} obtained with pure DME/DOL system.

We systematically studied the effect of the electrolyte volume in conventional Li–S electrolyte on capacity and Coulombic efficiency, and 25 μL turned out to be the optimal quantity (Fig. S1). In addition, the effect of the different additive proportions of DMTS on cycle performance was compared. Using the same amount of electrolyte (25 μL), the S/C cathodes tested in DMTS modified electrolytes show high initial specific discharge capacities (based on the weight of sulfur) of 1131.4, 1297.9, 1493.5, and 1361.1 mAh g^{-1} with various DMTS contents of 10, 20, 30 and 40 vol%, respectively, contrasting to 1018.6 mAh g^{-1} in pure DME/DOL cell at 0.1C (Fig. S2). Moreover, the rate performances of the S/C cathodes in conventional electrolyte and DMTS modified electrolytes were studied. Similarly, the optimal rate performance was also obtained with 30 vol% DMTS (Fig. S3). Control experiment was carried out as the identical condition using the conventional electrolyte, exhibiting a greatly decreased capacity values under 0.1C (1039.5 mAh g^{-1}), 1C (629.9 mAh g^{-1}) and 4C (250.0 mAh g^{-1}), analogous to most DME/DOL system. The enhanced capacity can be attributed to the high–efficiency utilization of active material because the sulfur occurred as radicals and reacted in DMTS electrolyte, facilitating the kinetically conversion of sulfur, which would be supported more fully in the sections to follow. Generally, higher DMTS ratio would result in more efficient utilization of active material and also higher capacity, which however, lead to worse ionic conductivity as shown in Fig. S4. By comparing the performances in different electrolytes with various DMTS contents, we can conclude that after increasing the DMTS ratio to 30 vol%, the impact on cell performance depends on ionic conductivity more significantly rather than kinetic conversion of sulfur. A further increase in DMTS content to 40 vol% resulted in a decrease in the discharge capacity and rate performance. The electrochemical impedance spectra (EIS) of cells assembled by different electrolyte showed very closed ohmic resistance (R_S) and interfacial charge transfer resistance (R_{CT}) except the one in 40 vol% DMTS (Fig. S5). The better stability of battery with the DMTS–containing electrolyte rather than with the conventional electrolyte was observed at the rate of 0.1C as shown in Fig. S6. All the cells assembled with DMTS additive electrolyte presented better stability than that without DMTS. It was further confirmed that the cell had the optimized cycling performance with 30 vol% DMTS, maintaining an extremely high discharge capacity of ~1074.2 mAh g^{-1} after 150 cycles, which was over twice the stable capacity of ~481.9 mAh g^{-1} in the conventional electrolyte. Comparing the performance of different DMTS contents, the optimal ratio of 30 vol% was studied further. The discharge/charge profiles were shown in Fig. S7 with 50 cycles, exhibiting a long discharge platform and great stability, which was consistent well with cyclic voltammetry experiments. Extended cycling at 2C rate was also conducted, illustrating the long–term cycle life over 838.8 mAh g^{-1} (Fig. 2d) and excellent Coulombic efficiency over 500 cycling periods. After cycling, the S/C cathode and Li anode were retrieved from the cell to investigate the morphology changes. The S/C cathode is integrity with negligible morphology evolution (Figs. S8a and S8b), and Li anode generally keeps smooth surface without obvious bumps and cracks (Fig. 1b), indicating the beneficial effect of DMTS additive on suppressing shuttle effect. As contrast, the cell cycled in pure DME/DOL electrolyte was disassembled and the original intact and uniform surface of S/C cathode changed into roughness (Fig. S8c). The cracks and bulk sulfur, accumulated aggregates of solid sulfur species, can be found everywhere, which is attributed to the dissolution and loss of sulfur. Meanwhile, Li surface is covered with mossy and bushy dendrites (Fig. 1c), which accelerates the failure of batteries.

The overall capacity of S/C cathode in 30 vol% DMTS modified electrolyte reaches up to 3.12 mAh when the sulfur loading was about 1.0 mg cm^{-2}, which is almost four times the capacity of DME/DOL system (Fig. S10) with the same volume of electrolyte (25 μL). Based on the mass of sulfur, the capacities of DMTS containing cells are 1.07, 1.26,

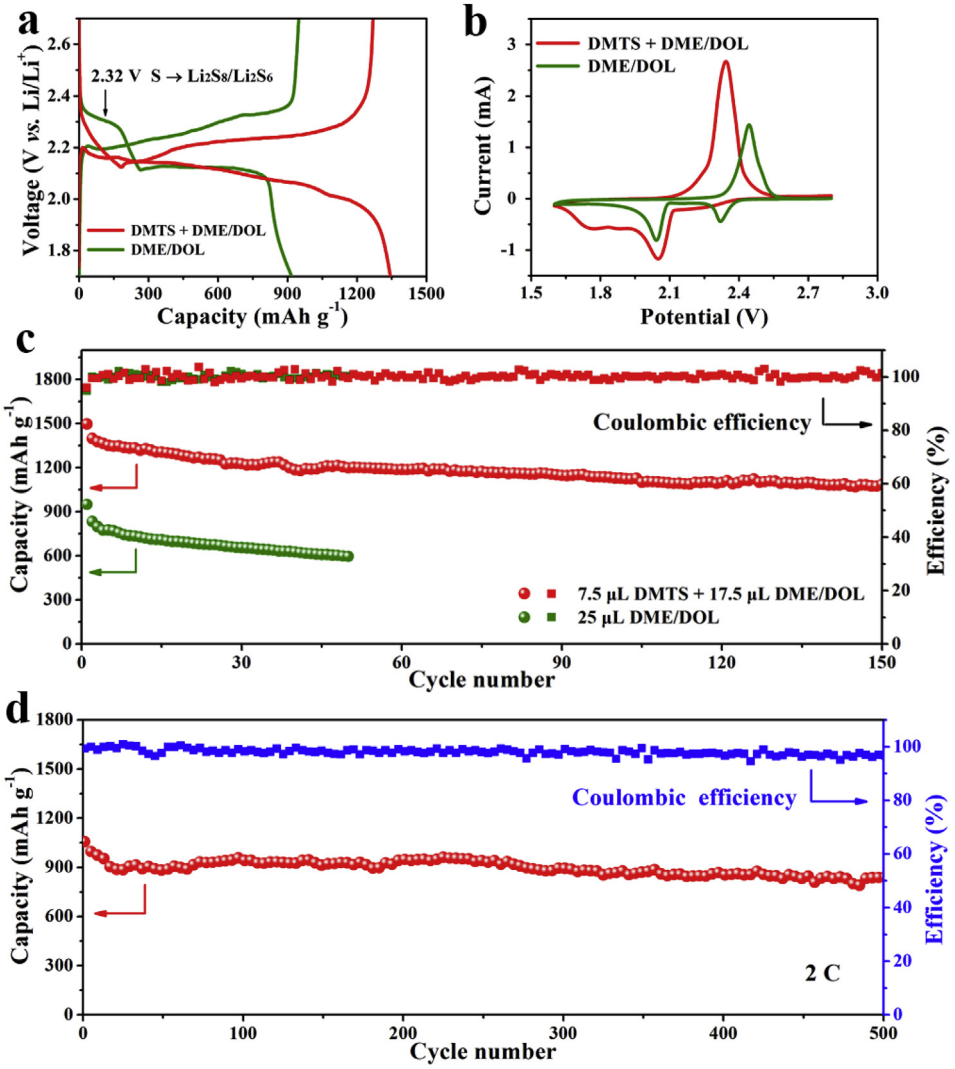

Fig. 2. (a) Comparsion of discharge/charge voltage profiles between conventional DME/DOL electrolyte and DMTS modified electrolytes with the same amount of electrolyte (25 µL). The 2.32 V discharge plateau, which should have corresponded to the conversion from solid S_8 to soluble polysulfide lithium (Li_2S_x, $4 \leq x \leq 8$) in conventional Li–S system, is not observed for the cells using DMTS modified electrolytes and instead it emerges a much longer plateau at ~2.08 V. (b) Cyclic voltammogram curves of two different cells, which is measured in a voltage range of 1.6–2.8 V at a scan rate of 0.1 mV s^{-1}. (c) The cell with 30 vol% DMTS additive electrolyte exhibits a much higher capacity than pure DME/DOL system. (d) Cycle life and coulombic efficiency of the cell with DMTS at 2C for long cycles.

1.42 and 1.29 mAh, respectively, with different DMTS contents of 10, 20, 30 and 40 vol%. Generally higher energy in DMTS modified cells than conventional DME/DOL cell is due to the radical exchange reaction, which stimulates the effective utilization of sulfur. The overall capacity was even up to 5.01, 7.62 and 8.67 mAh corresponding to high sulfur loading of 3.02, 5.88 and 8.12 mg cm^{-2}, respectively (Fig. 3a). The previous results of Li–S batteries [6,9,12,14,17,28–32] were shown for reference, and we calculated that the areal capacities based on the electrochemical data in Fig. 3a with respect to the mass of sulfur (Fig. 3b). Most reports showed a specific capacity of ~1 Ah g^{-1} while the sulfur loading was less than 4 mg cm^{-2}. Obviously, the capacity output of the S/C cathode in DMTS modified electrolyte was considerably higher

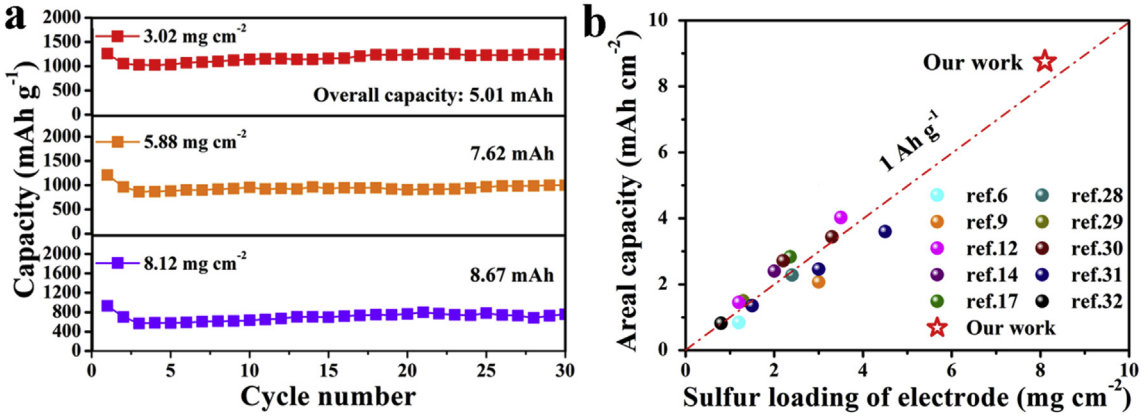

Fig. 3. (a) Cycle performance of the cells in 30 vol% DMTS modified electrolyte as the sulfur loading is 3.02, 5.88 and 8.12 mg cm^{-2} and the overall capacity is up to 5.01, 7.62 and 8.67 mAh, respectively. (b) Comparison of overall capacity and sulfur loading on the cathode with some previously reported Li–S cathodes.

than that in most previous reports. When the sulfur loading was up to 3.02 mg cm^{-2}, the discharge capacity of 1213.3 mAh g^{-1} can be still maintained after 150 cycles (Fig. S11), demonstrating that the cathodes exhibited great performance with high sulfur loading, which reveals potential application in future batteries.

To accurately evaluate the influence of DMTS on the electrochemical behavior of S/C electrode, NMR characterization at different states was carried out to monitor the intermediate process. Dimethyl thioether species were able to be identified by investigating ^{1}H NMR chemical shifts. Methyl proton resonances at $\delta = 2.48$ ppm for DMTS was clearly recognized by contrasting to the ^{1}H NMR signals of conventional electrolyte, where only constant peaks from DOL and DME can be observed as demonstrated in Fig. 4a. No extra peaks in the range of 2.4–2.7 ppm were observed after dissolving elemental sulfur into 30 vol% DMTS modified electrolyte, suggesting dimethyl polysulfides was not formed simply by dissolving elemental sulfur into DMTS, according with the results presented by DFT calculations (Fig. 1a). The ^{1}H NMR at different discharging states was used to validate the reduction pathway and reaction mechanism of DMTS modified electrolyte during cycling. Fig. 4c showed the spectra recorded at different depths of discharge, corresponding to the locations marked in Fig. 4b. During the initial discharge to 2.39 V, the peak strength of DMTS became weaker and the resonance peak at $\delta = 2.23$ ppm corresponding to the methyl group of DMDS appeared. At the same time, several peaks as the methyl group of dimethyl polysulfides ($\delta = 2.62$ ppm for $CH_3S_4CH_3$, $\delta = 2.70$ ppm for $CH_3S_5CH_3$, $\delta = 2.73$ ppm for $CH_3S_6CH_3$ and $\delta = 2.75$ ppm for $CH_3S_7CH_3$) arose [28], although keeping weaker signals compared to DMTS and DMDS. After further discharging, all these peaks became stronger and reached their maximum size at 2.10 V except DMTS. Subsequently, these peak intensities decreased simultaneously till the end of discharge, indicating gradually reduced concentrations of dimethyl thioether. In addition, the peaks between $\delta = 1.78$ ppm and 1.89 ppm were related to CH_3SLi, and the slight shift was supposed to the impact of complexation between the lone–pair electrons donated by the sulfur atom in CH_3SLi and the less electronegative lithium resulted from gradually increased Li_2S, with a binding energy of 0.49 eV according to DFT calculations. Herein, the mechanism for exchange reaction of radicals was proposed (Fig. S13a). The study on ^{1}H NMR convinced us that DMTS will cleave S–S bond, existing in $CH_3SS\bullet$ and $CH_3S\bullet$ radical forms during discharging process, which caused an obvious decrease at $\delta = 2.48$ ppm for DMTS. Although it was normally a non–spontaneous reaction to form dimethyl polysulfides according to the Gibbs free energy calculations, lithium–ion deriving from the cycle process of cells activated the radicals and resulted in the couple reaction of radical $CH_3S\bullet$ as certified by the appearance of DMDS. The exchange reaction between such activated radicals and DMTS caused the formation of dimethyl polysulfides as shown in ^{1}H NMR spectroscopy [33,34]. Before reaching at 2.10 V, the unreacted sulfur radicals involved in the radical reactions results in gradual increase in peak intensity for dimethyl thioether. Since active material was constantly reduced, thioether failed to recover efficiently, which caused a significant decrease in the concentration of DMTS and dimethyl polysulfides.

The intermediate discharged products are colored and can be detected by UV/Vis spectroscopy based on the principle of Beer–Lambert's law [35]. The general interaction between UV/Vis electromagnetic radiation and molecules of products can give absorption or reflection information of intermediates [35]. We applied *in–situ* UV/Vis spectroscopy to verify the discharge productions and the mechanism of sulfur reduction by monitoring the change of intermediates. A well–designed button cell, covered by the thin optical quartz glass, was built. The cathode and lithium plate were punched to make sure the signal reflected from separator can be recorded (seen in Fig. 5a). We studied *in–situ* UV/Vis spectra of cells in two different electrolytes with and without DMTS during discharge process. The absorption curves of S/C cathode in DMTS modified electrolyte and conventional Li–S electrolyte were revealed in Fig. 5b and d, respectively. The significant differences shown in two figures indicated different discharge mechanisms. In order to investigate the distinctions of discharged products more clearly, we respectively constructed their first–order derivatives of UV/Vis spectra and focused on their variations of peaks at different discharge voltage. The derivatives for DMTS free cell as shown in Fig. 5e exhibited a series of typical peaks and their shifts between 480 nm and 570 nm, which were attributed to the constant conversion from solid S_8 into high–order polysulfides then to low–order polysufides. Differ from that, the derivatives of S/C cell in

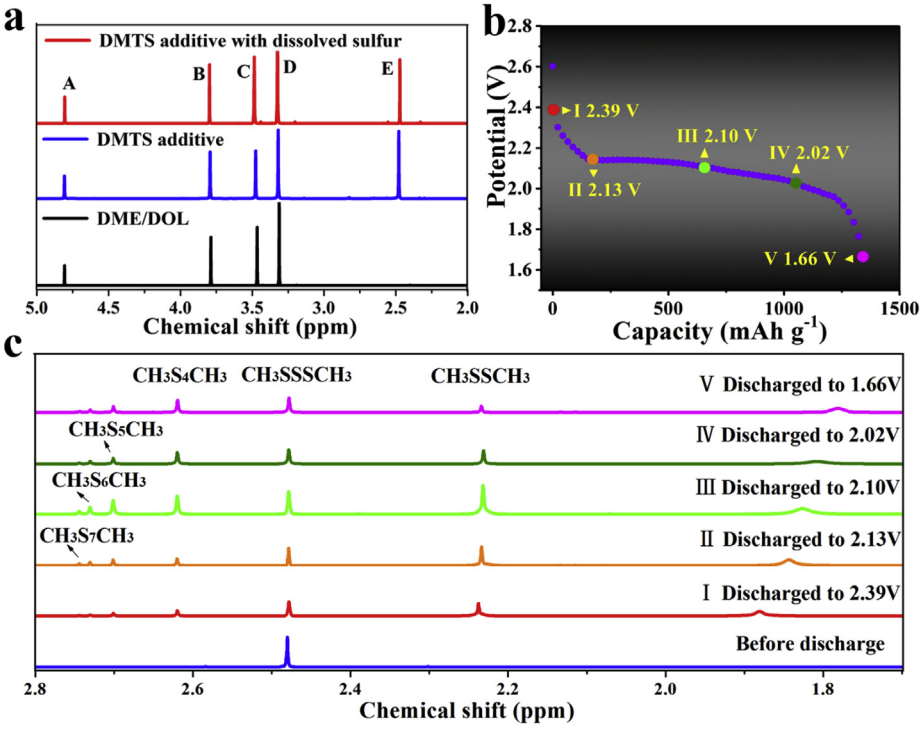

Fig. 4. (a) ^{1}H NMR spectra of DMTS modified electrolyte and a saturated mixture by dissolving sufficient elemental sulfur in the electrolyte at various discharge states. The major peaks at (A) 4.80 ppm and (B) 3.78 ppm attributes to DOL. (C) 3.48 ppm and (D) 3.29 ppm attributes to DME, DMTS modified electrolyte shows a major peak at (E) 2.48 ppm corresponding to DMTS. (b) Discharge profile of S/C cell in 30 vol% DMTS modified electrolyte cycled at 0.3C, corresponding to (c) The in operando ^{1}H NMR spectra at different discharge states.

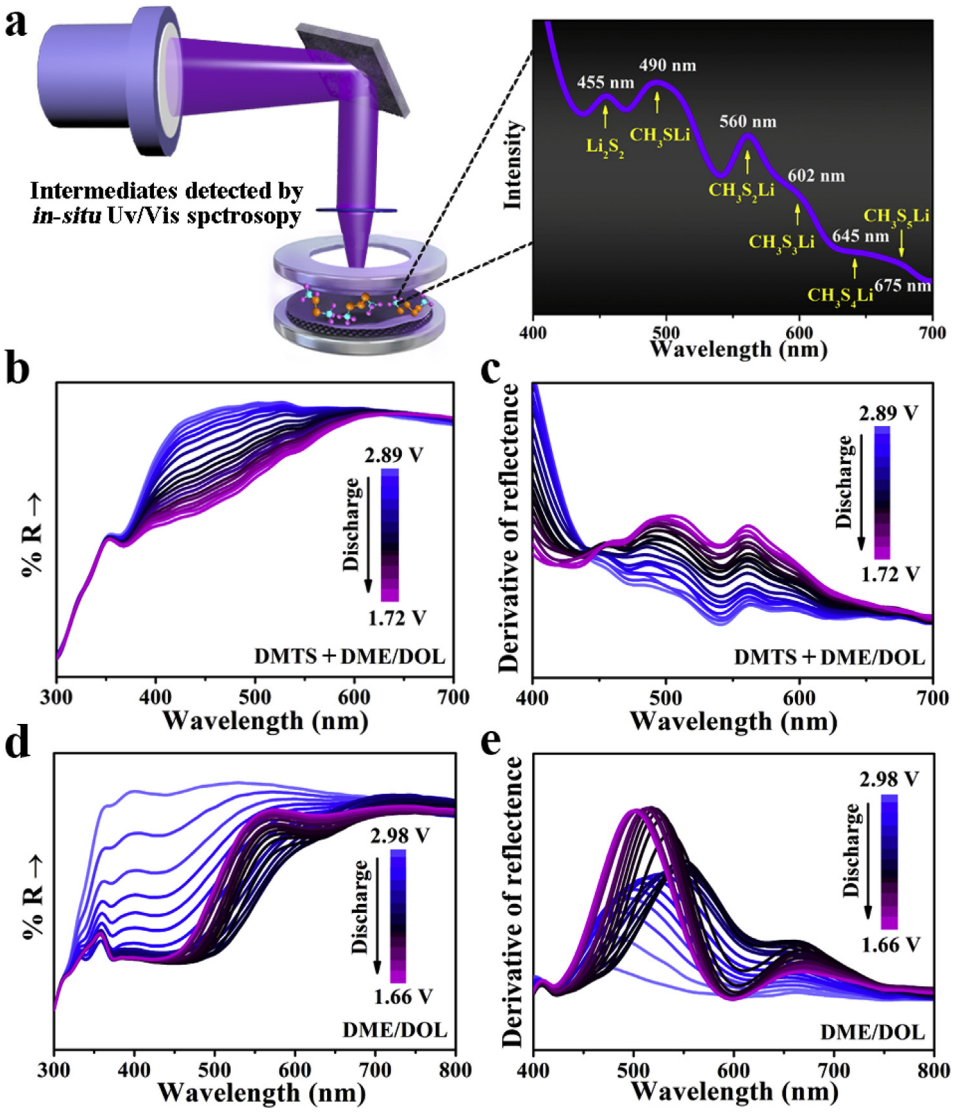

Fig. 5. (a) The model of well–designed cell used for *in–situ* UV/Vis spectra measurements. *In–situ* UV/Vis spectra of S/C cathode cycled in (b) 30 vol% DMTS modified and (d) conventional electrolyte during discharging process. First–order derivatives of *in–situ* UV/Vis spectra of S/C cathode cycled in (c) 30 vol% DMTS modified and (e) conventional electrolyte during discharging process.

DMTS modified electrolyte revealed six peaks labeled at ~455 nm, 490 nm, 560 nm, 602 nm, 645 nm and 675 nm, corresponding to Li_2S_2,CH_3SLi,CH_3S_2Li,CH_3S_3Li,CH_3S_4Li and CH_3S_5Li, respectively (Fig. 5a and c). The peaks exhibited the increase in intensities without location shifts during discharge. Furthermore, no evidence of long chain polysulfide lithium (Li_2S_x, $3 \leq x \leq 8$) was obtained according to the results in discharge intermediates. In addition, the weak peak of CH_3S_3Li, CH_3S_4Li and CH_3S_5Li ascribed to the small quantity of radical $CH_3S_n\bullet$ ($3 \leq n \leq 5$), which was well consistent with ^1H NMR spectroscopy and DFT calculations. Accordingly, we concluded that the radical $CH_3S_n\bullet$ ($1 \leq n \leq 3$) can react with Li^+ to form CH_3S_nLi ($1 \leq n \leq 3$), which transfers to CH_3SLi step by step without the formation of long–chain lithium polysulfides during the whole discharge process [15,36]. The charge process of the cell based on DMTS modified electrolyte was also recorded in Fig. S12. All peaks show gradually decrease in intensity during the cell charging, indicating the rapid disappear of dimethyl polysulfides, further demonstrating the reversible conversion of dimethyl sulfide intermediates upon delithiation, which also can be verified by the cell stable cycle performance with high capacity during repeated charging/discharging process. The general charge/discharge reaction mechanism during cycling is illustrated in Fig. S13b.

4. Conclusions

In summary, we have demonstrated a new strategy of using DMTS to realize dimethyl polysulfide intermediates, which are significant to increase the cell capacity and eliminate the shuttle effect efficiently. The cell delivered an initial specific capacity of 1497.3 mAh g^{-1}, and the overall capacity can even reach 8.67 mAh when the sulfur loading was increased to 8.12 mg cm^{-2}. Importantly, the as–prepared cell shows an excellent cycle performance with the capacity retention of 84.1% based on 500 cycles at the current rate of 2C. The result of DFT calculations demonstrates that DMTS exists in the most stable state in dimethyl thioether system. The sulfur on cathode electrode participated in the radical exchange reaction, preventing sulfur from routine reduction to lithium polysulfides, which was evidenced by NMR characterization at different discharge states and *in–situ* UV/Vis spectroscopy analysis. This work not only provides a strategy for enhancing the practical energy density of Li–S batteries, but also boosted the performance of sulfur cathodes by restricting the formation of soluble lithium polysulfides. The new reaction mechanism and prominent electrochemical performance set new trends and provided ideas for further research to advance high capacity Li–S battery technologies.

Acknowledgements

We acknowledge support from the National Natural Science Foundation of China (grants51622208, 21703149, and 51872193).

Appendix A. Supplementary data

Supplementary data to this article can be found online at https://doi.org/10.1016/j.ensm.2019.08.010.

References

[1] X.Y. Tao, J.G. Wang, C. Liu, H.T. Wang, H.B. Yao, G.Y. Zheng, Z.W. Seh, Q.X. Cai, W.Y. Li, G.M. Zhou, C.X. Zu, Y. Cui, Nat. Commun. 7 (2016) 11203.
[2] D. Liu, C. Zhang, G. Zhou, W. Lv, G. Ling, L. Zhi, Q.–H. Yang, Adv. Sci. 5 (2018) 1700270.
[3] Y. Yang, G.Y. Zheng, Y. Cui, Chem. Soc. Rev. 42 (2013) 3018–3032.
[4] Y. Zhong, X. Xia, S. Deng, D. Xie, S. Shen, K. Zhang, W. Guo, X. Wang, J. Tu, Adv. Mater. 30 (2018) 1805165.
[5] Y. Yang, Y. Zhong, Q. Shi, Z. Wang, K. Sun, H. Wang, Angew. Chem. Int. Ed. 130 (2018) 15775–15778.
[6] Z. Xiao, Z. Yang, L. Wang, H. Nie, M. Zhong, Q. Lai, X. Xu, L. Zhang, S. Huang, Adv. Mater. 27 (2015) 2891–2898.
[7] N. Xu, T. Qian, X. Liu, J. Liu, Y. Chen, C. Yan, Nano Lett. 17 (2017) 538–543.
[8] M. Wild, L. O'Neill, T. Zhang, R. Purkayastha, G. Minton, M. Marinescu, G.J. Offer, Energy Environ. Sci. 8 (2015) 3477–3494.
[9] Q. Zhang, Y. Wang, Z.W. Seh, Z. Fu, R. Zhang, Y. Cui, Nano Lett. 15 (2015) 3780–3786.
[10] C.–P. Yang, Y.–X. Yin, Y.–G. Guo, L.–J. Wan, J. Am. Chem. Soc. 137 (2015) 2215–2218.
[11] D. Moy, A. Manivannan, S.R. Narayanan, J. Electrochem. Soc. 162 (2015) A1–A7.
[12] M.S. Kim, L. Ma, S. Choudhury, L.A. Archer, Adv. Mater. Interfaces 28 (2016) 1600450.
[13] Y.S. Su, Y.Z. Fu, T. Cochell, A. Manthiram, Nat. Commun. 4 (2013) 2985.
[14] J. Jiang, J.H. Zhu, W. Ai, X.L. Wang, Y.Y. Wang, C.J. Zou, W. Huang, T. Yu, Nat. Commun. 6 (2015) 8622.
[15] M. Wu, Y. Cui, A. Bhargav, Y. Losovyj, A. Siegel, M. Agarwal, Y. Ma, Y. Fu, Angew. Chem. Int. Ed. 55 (2016) 10027–10031.
[16] S. Shen, X. Xia, Y. Zhong, S. Deng, D. Xie, B. Liu, Y. Zhang, G. Pan, X. Wang, J. Tu, Adv. Mater. 31 (2019) 1900009.
[17] J. Zhang, H. Hu, Z. Li, X.W. Lou, Angew. Chem. Int. Ed. 55 (2016) 3982–3986.
[18] H.–J. Peng, J.–Q. Huang, X.–B. Cheng, Q. Zhang, Adv. Energy Mater. 7 (2017) 1700260.
[19] Z. Li, L.X. Yuan, Z.Q. Yi, Y.M. Sun, Y. Liu, Y. Jiang, Y. Shen, Y. Xin, Z.L. Zhang, Y.H. Huang, Adv. Energy Mater. 4 (2014) 1301473.
[20] R.P. Fang, S.Y. Zhao, S.F. Pei, X.T. Qian, P.X. Hou, H.M. Cheng, C. Liu, F. Li, ACS Nano 10 (2016) 8676–8682.
[21] D. Gueon, J.T. Hwang, S.B. Yang, E. Cho, K. Sohn, D.–K. Yang, J.H. Moon, ACS Nano 12 (2018) 226–233.
[22] Z. Sun, J. Zhang, L. Yin, G. Hu, R. Fang, H.–M. Cheng, F. Li, Nat. Commun. 8 (2017) 14627.
[23] G. Zheng, Q. Zhang, J.J. Cha, Y. Yang, W. Li, Z.W. Seh, Y. Cui, Nano Lett. 13 (2013) 1265–1270.
[24] Y. Mao, G. Li, Y. Guo, Z. Li, C. Liang, X. Peng, Z. Lin, Nat. Commun. 8 (2017) 14628.
[25] H. Yi, T. Lan, Y. Yang, H. Zeng, T. Zhang, T. Tang, C. Wang, Y. Deng, Energy Storage Mater (2018), https://doi.org/10.1016/j.ensm.2018.12.009.
[26] W. Chen, T. Lei, T. Qian, W. Lv, W. He, C. Wu, X. Liu, J. Liu, B. Chen, C. Yan, J. Xiong, Adv. Energy Mater. 8 (2018) 1702889.
[27] S. Xu, Y. Cheng, L. Zhang, K. Zhang, F. Huo, X. Zhang, S. Zhang, Nano Energy 51 (2018) 113–121.
[28] S. Chen, F. Dai, M.L. Gordin, Z.X. Yu, Y. Gao, J.X. Song, D.H. Wang, Angew. Chem. Int. Ed. 55 (2016) 4231–4235.
[29] Z. Li, Y. Jiang, L.X. Yuan, Z.Q. Yi, C. Wu, Y. Liu, P. Strasser, Y.Y. Huang, ACS Nano 8 (2014) 9295–9303.
[30] X.B. Cheng, R. Zhang, C.Z. Zhao, F. Wei, J.G. Zhang, Q. Zhang, Adv. Sci. 3 (2016) 1500213.
[31] G.X. Li, J.H. Sun, W.P. Hou, S.D. Jiang, Y. Huang, J.X. Geng, Nat. Commun. 7 (2016) 10601.
[32] K.Y. Xie, Y. You, K. Yuan, W. Lu, K. Zhang, F. Xu, M. Ye, S.M. Ke, C. Shen, X.R. Zeng, X.L. Fan, B.Q. Wei, Adv. Mater. 28 (2016) 201604724.
[33] M. Fontecave, S. Ollagnier–de–Choudens, E. Mulliez, Chem. Rev. 103 (2003) 2149–2166.
[34] Y.L. Liang, Z.L. Tao, J. Chen, Adv. Energy Mater. 2 (2012) 742–769.
[35] M.U.M. Patel, R. Dominko, ChemSusChem 7 (2014) 2167–2175.
[36] S.Y. Wei, L. Ma, K.E. Hendrickson, Z.Y. Tu, L.A. Archer, J. Am. Chem. Soc. 137 (2015) 12143–12152.